7-5-2016

Generation of simple extended porous surface expression from results of pore-level conjugate heat transfer in spherical-void-phase porous blocks

Anthony G. Straatman
Western University, agstraat@uwo.ca

Alex Kalopsis
Western University

Nolan Dyck
Western University

Proceedings of the 6th International Conference on Porous Media and Its Applications in Science and Engineering
ICPM6
July 3-8, 2016, Waikoloa, Hawaii

GENERATION OF SIMPLE EXTENDED POROUS SURFACE EXPRESSION FROM RESULTS OF PORE-LEVEL CONJUGATE HEAT TRANSFER IN SPHERICAL-VOID-PHASE POROUS BLOCKS

Anthony G. Straatman, Alex Kalopsis and Nolan Dyck

Department of Mechanical & Materials Engineering
Western University, London, Ontario, N6A 5B9, Canada

ABSTRACT

Pore-level calculations of highly-conductive spherical-void-phase foams are performed to facilitate the calibration of a simple one-dimensional extended-surface model for porous heat sinks. Convective heat transfer coefficients are derived from isothermal calculations of several geometric models over a range of flow Reynolds numbers. The extended-surface model considers the stream wise variation of temperature in its derivation and utilizes a modified expression for the fin parameter *m*. Additional pore-level calculations are then done for cases where the porous blocks are attached to a heated substrate. For these cases, fully conjugate calculations are performed to predict the heat transfer from the substrate. These calculations are compared to predictions obtained from the one-dimensional extended surface model, where it is shown that estimates to within 5% can be made under most conditions considered. It is noted that consideration of conduction effects may further improve the formulation.

INTRODUCTION

Studies of convection in porous media continue to be of interest due to the increasing utility of highly-conductive porous materials in heat exchange applications. Permeable porous foams have emerged as a viable heat sink material due to their large internal surface area and high interstitial heat exchange that results from the tortuous path taken by the fluid as it traverses the internal structure of the foam.

Several authors have studied Aluminum foams both experimentally and numerically to characterize the heat transfer and pressure penalty. Antohe et al. [1], Paek et al. [2], and Boomsma & Poulikakos [3] present results of hydraulic losses of normal and compressed aluminum foams to quantify the permeability and form drag coefficients for foams of different porosity and material properties. Calmidi and Mahajan [4] studied forced convection in highly porous aluminum foams using experiments and computational fluid dynamics. Their paper reports on hydraulic losses, interstitial exchange, and thermal dispersion. In general, aluminum foams have a highly porous structure (92-96% void) that enables fluid to pass through relatively easily, resulting in modest heat transfer enhancement, but with little pressure penalty.

Another conductive foam that has received significant attention as a potential heat transfer material is graphitic foam [5,6]. Cast or foamed materials like graphitic foam also have an open, interconnected void structure that enables fluid exposure to internal surface area and thus the potential for significant convective heat transfer, however, at a higher pressure penalty. Such materials also have the potential for wide application in energy exchange and heat recovery. Graphitic foam has an effective (stagnant) conductivity on the order of 40-160 [W/m K] [5] due to the high conductivity of the graphitized carbon material (800-1900 [W/m K]). To compare, similar porosity aluminum foams have effective conductivities on the order of 2-26 [W/m K], resulting from conductivities of 140-237 W/m K for various aluminum alloys [2]. The high conductivity of the graphitized solid enables the foam to readily entrain heat from a substrate into the solid structure of the foam producing significant thermal no-equilibrium making it useful as a heat transfer material.

No matter the porous material under consideration, there is a need for modelling the flow and heat transfer with high accuracy in a manner that is computationally inexpensive. There exists a range of approaches that can be used for simulation starting from pore-level calculations of fluid flow and energy exchange, to volume-averaged approaches, which consider the porous media as a porous continuum. To bridge the gap between these two approaches, pore-level calculations are often performed on a small representative elemental volume (REV) of porous foam, which are then used to derive coefficients that are required to close the volume-averaged

equations [7]. While pore-level calculations are only possible for small REVs, volume-averaged correlations can be used to study complete heat exchange devices within the framework of conjugate fluid/porous/solid codes [8,9].

It is also of interest to develop a simple extended-surface model for porous media that can be used for basic analytical heat transfer calculations. Such a model was originally developed in [10] to account for the enhanced equivalent conductivity in a foam-filled heat sink, but without specific verification with experiments or detailed simulations. In the present work, a unique geometric model [11] is used to generate several spherical-void-phase (SVP) geometries of different porosity and pore diameter. These geometric models are discretized and both isothermal and conjugate results of heat and fluid flow are obtained using the commercial software CFX [12]. The isothermal results are used in the formulation of a one-dimensional extended surface model, which is then used to predict the heat transfer from foam blocks of different solid-phase conductivity attached to a heated substrate. Comparison of heat transfer results to similar results obtained from the detailed conjugate simulations demonstrate the viability of the simple analytical approach to conducting heat transfer calculations.

NOMENCLATURE

A	=	Internal area of REV [m^2]
A_c	=	Cross-sectional area at substrate [m^2]
A_{sf}	=	Area per unit volume of REV [m^2/m^3]
C_P	=	Specific heat [W/kg K]
d_p	=	Pore diameter [μm]
h_{sf}	=	Interstitial heat transfer coefficient [W/m^2 K]
k, k_s	=	Conductivities of fluid & solid [W/m K]
k_{eq}	=	Equivalent conductivity [W/m K]
L	=	Length of heated section [m]
L_e	=	Side length of REV [m]
$\dot{m}$	=	Mass flux through REV [kg/s]
Nu_{dp}	=	Interstitial Nusselt number
P_{xy}	=	Foam perimeter in plane normal to Substrate surface [m]
P_{xz}	=	Foam perimeter in plane normal to air flow [m]
Q	=	Heat transfer [W]
Re_{dp}	=	Reynolds number ($=\dot{m}d_p/\mu L_e^2$)
T_{mi}	=	Bulk inlet temperature [K]
T_{mo}	=	Bulk outlet temperature [K]
T_s	=	Solid-phase temperature [K]
T_w	=	Substrate temperature [K]
V	=	Volume of REV [m^3]
x,y,z	=	Principle coordinates

Greek Symbols

ε	=	Porosity of REV (void fraction)

Subscripts

sf	=	Solid-fluid interface

1 Pore-level Calculations

Pore-level calculations have been carried out in this study for two purposes; first to determine the interstitial convective heat transfer coefficient as a function of flow and geometry for cases where the SVP is considered isothermal, and second for cases where the SVP block is considered to be attached to a solid substrate transferring heat as a heat sink. In the first case, only the void portion of the REV requires discretization and simulation, while in the second case, the fluid and solid constituents must be discretized and solved simultaneously. Results of the second set of calculations are used to verify the accuracy of a one-dimensional extended surface model for SVP foams that utilizes the interstitial coefficients derived from the first set of calculations.

The geometric tool described in [11] was used to generate representative elemental volumes of SVP foams. The geometric tool requires specification of the number and size of pores (primitives) to be included in the volume; the tool initially places the primitives in a random pattern within a large cubic volume and then mathematically "squeezes" the cube until the target porosity is reached. During the "squeezing" operation, the pores move within the domain in response to a mathematical contact law, and eventually intersect each other to a certain measure of interference based on the force balance. The result is a random SVP domain that has a specified pore diameter and porosity. A particularly unique feature of this digital domain generation tool is that it enforces spatial periodicity in all three principle directions and thus, the resulting REV can also be used as a building block in any direction to produce larger domains of the same geometric properties.

Figure 1 shows an image of a typical SVP foam generated using [11], while Fig. 2 compares a digitally generated SVP foam with SEM images of graphitic foam. As illustrated, the digitally generated foams are an excellent replication of the graphitic structure in terms of the randomness of the pore orientation and the pore windows that connect the pores.

Geometric models were produced for four porosities (0.70, 0.75, 0.80, 0.85), and two pore diameters (400, 800μm). In generating the geometric models, several cases were run with different numbers of primitives to be sure that results of heat and fluid flow were independent of the model dimensions. The study indicated that geometric models with 100 primitives was suitable for all cases considered. Table 1 gives a summary of the REVs used herein along with all relevant geometric properties. In Table 1, d_P is the pore diameter in μm, L_e is side length of the REV in [m], V is the total volume of the REV in [m^3], A is the internal surface area of the REV in [m^2], A_{sf} is the area per unit volume in [m^2/m^3], and ε is the porosity, which is defined as the void volume per total REV volume. The final column gives a dimensionless quantity based on the foam parameters.

Table 1: Summary of geometric parameters for representative elemental volumes (REV) of SVP foams generated for the pore-level calculations of heat and fluid flow.

REV #	d_p [μm]	L_e [m]	V [m^3]	A [m^2]	A_{sf} [m^2/m^3]	ε	$\varepsilon/d_p A_{sf}$
1	400	0.002111	9.41e-09	8.40e-05	8924	0.70	0.196
2	400	0.002054	8.67e-09	7.63e-05	8807	0.75	0.213
3	400	0.001999	7.99e-09	6.81e-05	8517	0.80	0.235
4	400	0.001943	7.33e-09	5.79e-05	7898	0.85	0.269
5	800	0.004205	7.44e-08	3.14e-04	4222	0.70	0.207
6	800	0.004091	6.85e-08	2.90e-04	4233	0.75	0.221
7	800	0.003971	6.26e-08	2.50e-04	3999	0.80	0.250
8	800	0.003855	5.73e-08	2.13e-04	3721	0.85	0.286

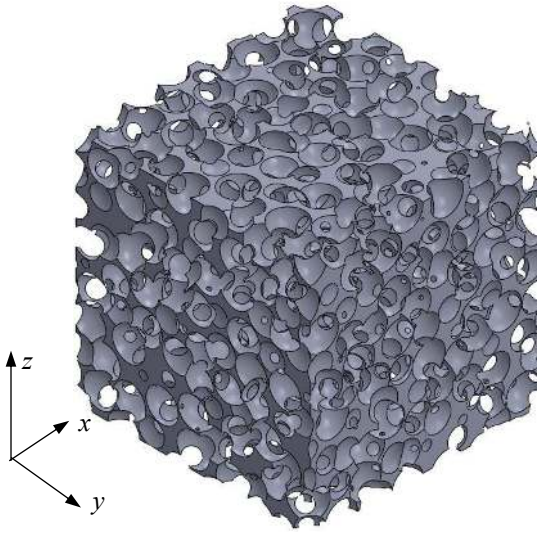

Figure 1: Digital representation of SVP foam generated using 600 primitives [11].

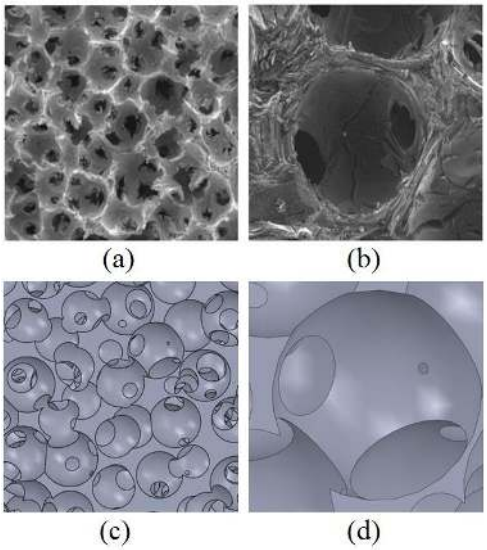

Figure 2: SEM images of a graphite foam specimen (a) and (b) [13] in comparison to a CAD model of the SVP geometry generated using the method of [11] (c) and (d).

The SVP geometries were meshed using the ANSYS meshing tool to produce tetrahedral grids that were fine near solid boundaries and gradually increased towards the pore centers.

1.1 Isothermal solid

Calculations were first conducted on all 8 REVs indicated in Tab. 1 to simulate flow and convective heat transfer under isothermal conditions. For these cases, only the fluid constituent of the REV required meshing, and grids of 16,770,000 tetrahedral elements were required to produce grid-independent solutions to better than 5% based on total heat transfer and pressure drop.

The commercial CFD software ANSYS CFX [12] was used to run simulations of airflow through the SVP models. In all cases, the flow was considered laminar and advection in the momentum and energy equations was modelled using second-order up-winding. Steady-state simulations were run to residual levels of 10^{-6}. The boundary conditions for the isothermal cases were that of periodicity in all three principle directions, with the specification of a mass flow rate in the x-direction; and isothermal conditions for the interior surfaces. A temperature difference of 20 [K] between the solid and the incoming fluid was used for all calculations.

Figure 3 shows the results of the isothermal simulations in terms of interstitial Nusselt number, which was formulated by consideration of the temperature difference through the foam:

$$\frac{T_s - T_{mo}}{T_s - T_{mi}} = \exp\left(-\frac{h_{sf} A}{\dot{m} C_P}\right), \qquad [1]$$

where T_s is the solid-phase (interface) temperature, T_{mo} is the bulk outlet temperature, T_{mi} is the bulk inlet temperature, h_{sf} in the interstitial heat transfer coefficient, and C_P is the heat capacity of the fluid. Solving Eq. 1 for the interstitial heat transfer coefficient gives:

$$h_{sf} = -\left(\frac{\dot{m} C_P}{A}\right) ln\left(\frac{T_s - T_{mo}}{T_s - T_{mi}}\right), \qquad [2]$$

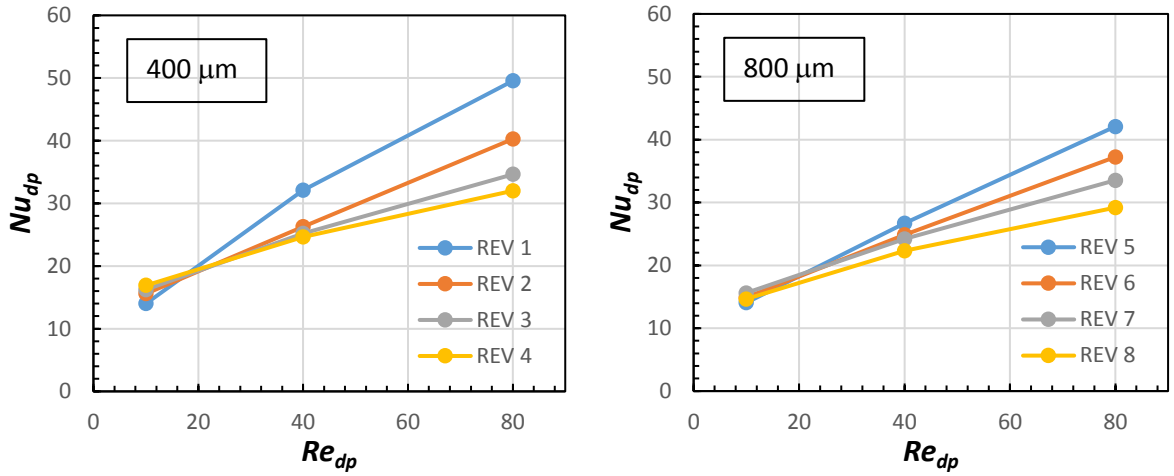

Figure 3: Nusselt number Nu_{dp} as a function of Re_{dp} for all pore-level isothermal simulations.

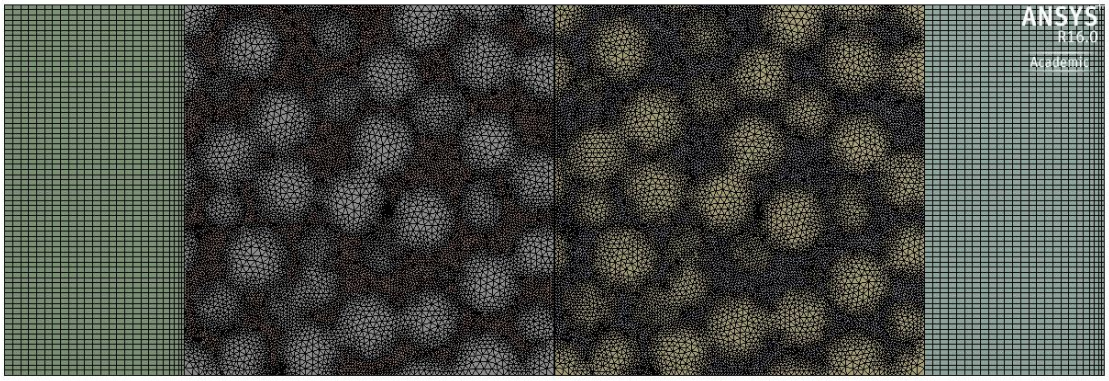

Figure 4: Planar (x-z) cross-section of computational domain and mesh for conjugate case of d_p= 400µm and ε= 0.75 (REV 2 in Table 1).

which is combined with the area per unit volume and the pore diameter to give the expression used for the Nusselt number:

$$Nu_{dp} = \frac{A_{sf} h_{sf} d_p^2}{k}, \qquad [3]$$

where k is the fluid conductivity. Figure 2 shows that the heat transfer increases in all cases with Re_{dp}, but the exponential nature of the Nusselt number variation decreases with increasing $\varepsilon/d_p A_{sf}$. Note that $\varepsilon/d_p A_{sf}$ is a dimensionless geometric group that characterizes the spherical void structure (see Table 1). No single correlation describing the Nusselt number for the isothermal cases is proposed herein, mainly because of the small number of cases run and the Reynolds number range considered. This is not to say that such a correlation is not possible; the correlation is clearly a function of all of the geometric parameters, as is evident in Fig. 3, and may be developed in terms of the dimensionless group $\varepsilon/d_p A_{sf}$. In the present study, the results for the interstitial heat transfer coefficient (Eq. 2) are used directly in the formulation of the simplified extended surface model.

1.2 Conjugate heat transfer

For the second part of the pore-level study, the REVs were assumed to be attached to a solid substrate and conjugate calculations were done to predict the flow and convective heat transfer from the foam and base combined. Pure-fluid inlet and outlet sections were added to the domain such that the porous region was treated as a heat sink. In all cases, a double-long REV was used. The domain was a three-dimensional channel of cross-section $L_e \times L_e$, and length $3L_e$ (in the x-direction) with a porous plug of length $2L_e$ positioned $0.5L_e$ from the inlet plane; Fig. 4 shows a center-plane (x-z) cross-section of the domain for one case illustrating the inlet and outlet sections and the grid distribution. As both the void and solid constituents of the REV required meshing, grids comprised of approximately 31,230,000 elements were necessary to produce grid-independent results to within 5%.

The boundary conditions were that of periodic conditions on the lateral y planes, a symmetry condition on the upper z plane, and a wall condition on the lower z plane; where the REV is in contact with the lower z plane, a temperature is imposed, while the remainder of the lower plane (the pure-fluid sections) is specified as adiabatic. The temperature difference between the incoming fluid and the substrate was fixed at 20 [K] for all cases. Computations of conjugate heat transfer were carried out for REVs 2, 4, 6 and 8 (see Table 1) and each for solid-phase conductivities of 50, 100, 200 and 400 [W/m K], and

Reynolds numbers of 10, 40 and 80, for a total of 24 cases. Fringe plots of the solid- and fluid-phase temperatures on the center plane are given in Fig. 5 for the case of d_p= 400µm, ε= 0.75, k_s= 100 [W/m K] and Re_{dp}= 80 (only results for the foam portion of the domain are shown). The images show that both the solid and fluid temperatures vary substantially through the domain in both the stream wise (x) direction and the vertical (z) direction due to the temperature difference imposed between the substrate and the incoming air. The air warms gradually from the foam inlet to outlet due to thermal non-equilibrium.

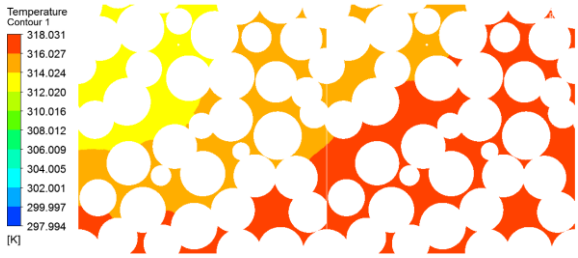

(a) Temperature distribution in solid phase

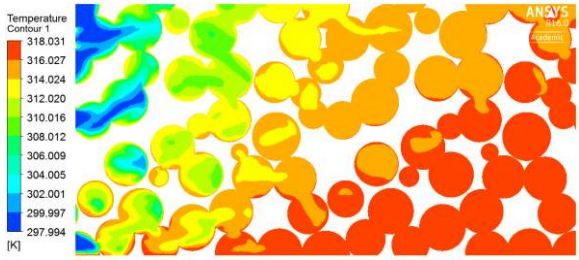

(b) Temperature distribution in fluid phase

Figure 5: Temperature distributions on the center (x-z) plane for the conjugate case where d_p= 400µm, ε= 0.75, k_s= 100 [W/m K] and Re_{dp}= 80.

2 Extended surface model

The extended surface model first described in [10] is adopted herein to test its ability to predict heat transfer from porous heat sinks. The central notion of the extended-surface model is that the fluid-solid temperature difference needs to vary as fluid passes through the foam structure. To this end, if we consider that heat sink materials are often highly conductive, a simple estimate of the fluid-solid temperature variation through the foam can be derived from the log-mean temperature difference, ΔT_{LM} defined as:

$$\Delta T_{LM} = \frac{(T_s - T_{mi}) - (T_s - T_{mo})}{ln\frac{(T_s - T_{mi})}{(T_s - T_{mi})}} \quad [4]$$

Since it is the temperature at the outlet of the foam block that is not known, a form of Eq. 1 can be used except with the internal area replaced with the product of perimeter and foam length:

$$\frac{T_s - T_{mo}}{T_s - T_{mi}} = \exp\left(-\frac{h_{sf} P_{yz} L}{\dot{m} C_P}\right) \quad [5]$$

where P_{yz} is an estimate of the perimeter at a cross-section normal to the airflow. The perimeter can be estimated by considering that the total internal area of the foam, A ($=A_{sf}V$) can be expressed as the product of a cross-sectional perimeter and REV height L_e. This gives:

$$P_{yz} = A_{sf} L_e^2 + \varepsilon L_e \quad [6]$$

where the first term is the perimeter of the foam structure and the second term is the additional perimeter due to the presence of the heated base. An estimate of perimeter is also required for the heat flow normal to the substrate, which is given as:

$$P_{xy} = A_{sf} L_e L \quad [7]$$

where L is the foam length in the stream wise (x) direction. An expression for the volume-averaged solid-phase temperature can now be derived starting from a slightly modified form of the basic differential equation for fins:

$$\frac{d^2 T_s}{dz^2} - \frac{h_{sf} P_{xy}}{k_{eq} A_c}(T_s - T_\infty) = 0 \quad [8]$$

where T_s is the solid phase temperature, T_∞ is the fluid temperature, $k_{eq} = \varepsilon k + (1-\varepsilon)k_s$ is the equivalent conductivity of the foam in the direction normal to the heated substrate, and A_c is the cross-sectional area at the REV-substrate interface. To incorporate the varying fluid-solid temperature difference within the foam, T_∞ is introduced as a bulk temperature that varies with the flow direction as:

$$T_\infty = T_m(x) \quad [9]$$

Then, incorporating Eq. 5 with T_{mo} replaced by $T_m(x)$ and L replaced by x, we can recast Eq. 8 as:

$$\frac{d^2 T_s}{dz^2} - \frac{h_{sf} P_{xy}}{k_{eq} A_c}(T_s - T_{mi})\exp\left(-\frac{h_{sf} P_{yz} x}{\dot{m} C_P}\right) = 0 \quad [10]$$

This equation can now be integrated with respect to the flow direction (x) and then divided by the flow length of the heat sink (L) to give:

$$\frac{d^2 T_s}{dz^2} + \frac{\dot{m} C_P P_{xy}}{k_{eq} A_c L P_{yz}}\left[\exp\left(-\frac{h_{sf} P_{yz} L}{\dot{m} C_P}\right) - 1\right] T_s = 0 \quad [11]$$

which, if taken in the conventional form of:

$$\frac{d^2 T_s}{dz^2} - m_p^2 T_s = 0, \quad [12]$$

an expression for the extended-surface parameter m_p emerges as:

$$m_p = \sqrt{\frac{\dot{m} C_P P_{xy}}{k_{eq} A_c L P_{yz}}\left[1 - \exp\left(-\frac{h_{sf} P_{yz} L}{\dot{m} C_P}\right)\right]} \quad [13]$$

which is similar to that derived in Ref. [10], with the exception of the definitions of A_c and T_s. Finally, making the adiabatic-tip fin assumption, the solution to Eq. 12 is:

$$\frac{T_s(z)-T_\infty}{T_w-T_\infty} = \frac{\cosh[m_p(L_e-z)]}{\cosh m_p L_e} \qquad [14]$$

The solution for the heat transfer from the foam heat sink can then be computed as:

$$Q = -k_{eq} A_c \left.\frac{dT_s}{dz}\right|_{z=0} \qquad [15]$$

$$Q = k_{eq} A_c m_p (T_w - T_\infty) \tanh m_p L_e \qquad [16]$$

While in Ref. [10] Eq. 13 was used to obtain accurate estimates of k_{eq} given Q and m_p, in the present treatment, the value of m_p is computed directly from Eq. 13 using known quantities, and the heat transfer is computed from Eq. 16.

Comparisons of the conjugate calculations with the estimates from Eq. 16 are given in Fig. 5, which shows the heat transfer predicted from the conjugate simulations on the abscissa and the heat transfer estimated from Eq. 16 on the ordinate. The figure shows an excellent agreement between the results for most of the range considered. The largest differences occur for the 800μm foam at 85% porosity, but only for the highest Reynolds numbers considered.

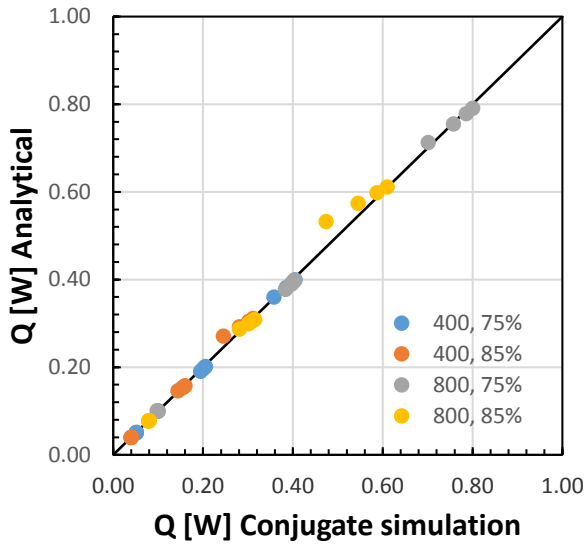

Figure 5: Comparison of heat transfer from conjugate computations to analytical estimates from Eq. 16.

CONCLUSIONS

A simple extended-surface model is formulated using results for interstitial convective exchange derived from pore-level isothermal simulations of several SVP models of porous foam. Results for heat transfer estimated from the simple analytical model are compared to similar results derived from detailed simulations of pore-level conjugate heat transfer. The results are in excellent agreement over the range of parameters considered with most results being within 5%. The larger differences (up to 20%) at high porosity are attributed to longitudinal conduction effects that have not been considered in the simplified model.

ACKNOWLEDGEMENT

The authors gratefully acknowledge financial support from the Natural Sciences and Engineering Research Council of Canada (NSERC).

REFERENCES

[1] Antohe, B. V., Lage, J. L., Price, D. C., and Weber, R. M., 1997, "Experimental Determination of Permeability and Inertia Coefficients of Mechanically Compressed Aluminum Porous Matrices," ASME J. Fluids Eng., 119, pp. 404–412

[2] Paek, W. J., Kang, H. B., Kim, Y. S., and Hyum, M. J., 2000, "Effective Thermal Conductivity and Permeability of Aluminum Foam Materials," Int. J. Thermophys., **21**(2), pp. 453–464.

[3] Boomsma, K., and Poulikakos, D., 2002, "The Effects of Compression and Pore Size Variations on the Liquid Flow Characteristics in Metal Foams," ASME J. Fluids Eng., 124, pp. 263–272.

[4] Calmidi, V. V., and Mahajan, R. L., 2000, "Forced Convection in High Porosity Metal Foams," ASME J. Heat Transfer, 122, pp. 557–565.

[5] Klett, W. J., Hardy, R., Romine, E., Walls, C., and Burchell, T., 2000, "High-Thermal Conductivity, Mesophase-Pitch-Derived Carbon Foam: Effect of Precursor on Structure and Properties," Carbon, 38, pp. 953–973.

[6] Gallego, C. N., and Klett, W. J., 2003, "Carbon Foams for Thermal Management," Carbon, 41, pp. 1461–1466.

[7] DeGroot, C. T., Straatman, A. G., "Numerical results for the effective flow and thermal properties of idealized graphitic foam," *ASME J. Heat Transfer*, 134(4), Article 042603, 2012.

[8] Betchen, L. J., Straatman, A. G., Thompson, B. E., "A Non-Equilibrium Finite-Volume Model for Conjugate Fluid/Porous/Solid Domains," *Numerical Heat Transfer, Part A*, 49, 543-565, 2006.

[9] DeGroot, C. T., Straatman, A. G., "A finite-Volume model for fluid flow and non-equilibrium heat transfer in conjugate fluid-porous domains using general unstructured grids," *Numerical Heat Transfer Part B*, 60(4), 252-277, 2011.

[10] C. T. DeGroot, A. G. Straatman, L. J. Betchen, "Modelling forced convection in finned metal foam heat sinks," *ASME J. Electronic Packaging*, (131), 021001-1 – 021001-10, 2009.

[11] N. J. Dyck, A. G. Straatman, "A new approach to digital generation of spherical void phase porous media microstructures," *Int. J. Heat and Mass Transfer*, (81), 470-477, 2015.

[12] CFX-ANSYS, Copyright 2015.

[13] J. W. Klett. *Process for Making Carbon Foam* 2000.